Proceedings of the ASME 2010 International Mechanical Engineering Congress & Exposition
IMECE2010
November 12-18, 2010, Vancouver, British Columbia, Canada

IMECE2010-40525

STUDY OF STRONG PRESSURE WAVE PROPAGATION IN A TWO-PHASE BUBBLY MIXTURE

Reni Raju
DYNAFLOW, INC.
www.dynaflow-inc.com
10621-J Iron Bridge Road, Jessup, MD, USA
reni@dynaflow-inc.com

Sowmitra Singh
DYNAFLOW, INC.
www.dynaflow-inc.com
10621-J Iron Bridge Road, Jessup, MD, USA
sowmitra@dynaflow-inc.com

Chao-Tsung Hsiao
DYNAFLOW, INC.
www.dynaflow-inc.com
10621-J Iron Bridge Road, Jessup, MD, USA
ctsung@dynaflow-inc.com

Georges Chahine
DYNAFLOW, INC.
www.dynaflow-inc.com
10621-J Iron Bridge Road, Jessup, MD, USA
glchahine@dynaflow-inc.com

ABSTRACT

A geometrically simple configuration of a gas bubble expanding in a bubbly medium is chosen to study multi-scale modeling approaches in simulating multiphase flows. Three solvers following the Eulerian-Lagrangian, multi-component compressible and analytical approaches have been studied for different bubbly medium void fractions. In the Eulerian-Lagrangian approach, an incompressible solver was coupled with a bubble dynamics model, while for the Eulerian two-fluid approach and the analytical model the surrounding fluid was assumed to be a homogeneous mixture. It was found that both two-fluid and analytical models match very well for the cases tested. The Eulerian-Lagrangian model shows that the dynamics of the bubbly medium and the expanding bubble are inherently coupled in a non-linear fashion. Presence of discrete bubbles also introduces localized perturbations in the void fraction as well as in the pressure distribution which cannot be captured by the homogeneous mixture models.

INTRODUCTION

Two phase flows are usually modeled using two broad classes of methods: the Lagranian-Eulerian approach, wherein one phase is modeled as discrete particles while the second phase is solved in an Eulerian fashion; or the continuum approach, where both phases are treated either as an equivalent single medium with equivalent properties as two fluids with different properties and interaction forces between them [1,2]. The first class of methods is especially useful for particle-laden flows as well as for droplets or bubbly flows [3,4,5] where by resolving the forces on each of the physical particles the corresponding equations of motion and other properties can be solved for. The latter method is useful for dispersed phase e.g. low void fraction bubbly flows [6,7,8].

In reality there are many practical applications where representing a bubbly two-phase medium as a continuum [9,10,11] where the bubbles just provide their compressibility to modify the liquid behavior is not totally adequate. For applications involving physical phenomena such as cavitation and/or propagation of shock and pressure waves in the bubbly medium, the bubbles' dynamics, motions and deformations, and their resulting feedback and modification of the liquid flow are essential. Alternatives to this approach require multi-scale type methods which are based on simultaneous and detailed description of all these effects.

In this paper we present a set of intermediary practical approaches and consider a geometrically simple but challenging numerical configuration for validation and evaluation of the applicability region of each method. The models are based on coupling Eulerian approaches for the equivalent two-phase medium and Lagrangian approaches for the bubbles. Two different liquid models are considered: one is viscous with density variation in time, and the other is multi-medium and compressible. The Lagrangian modeling of the bubbles includes the options to include or ignore bubble motion and bubble interaction.

We consider as a test case the pressure and flow field generated by the spherical dynamics of a relatively large bubble embedded in a bubbly mixture composed of much finer

bubbles. Within this framework we explore the accuracy and limitations of each method. Various conditions of bubble sizes and void fractions are considered and their effects are investigated. The two-way effects of the presence of the bubbles on the large bubble dynamics and on the propagation of pressure waves in the medium and on the distribution in space and time variation of void fraction in the domain are described. In addition an analytical model for predicting spherical dynamics of a large bubble in a bubbly mixture is used and compared with the numerical approaches.

NUMERICAL METHODOLOGY

Viscous Flow Solver with Density Variations

The unsteady Navier-Stokes equations for a liquid-gas mixture written in non-dimensional form are as follows:

$$\frac{\partial \rho_m}{\partial t} + \frac{\partial \rho_m u_i}{\partial x_i} = 0 \tag{1}$$

$$\frac{\partial \rho_m u_i}{\partial t} + \frac{\partial \rho_m u_i u_j}{\partial x_j} = -\frac{\partial p}{\partial x_i} + \frac{\partial}{\partial x_j}\left[\upsilon_m\left(\frac{\partial u_i}{\partial x_j} + \frac{\partial u_j}{\partial x_i}\right)\right] - \rho_m \delta_{i3}\frac{1}{\mathrm{F_r}^2} \tag{2}$$

Here, ρ_m is the mixture density, u its velocity, p its pressure, υ_m its kinematic viscosity and $\mathrm{F_r}$ is the Froude number. The mixture density and viscosity can be defined as,

$$\begin{aligned} \rho_m &= (1-\alpha)\rho_l + \alpha\rho_g \\ \upsilon_m &= (1-\alpha)\upsilon_l + \alpha\upsilon_g \end{aligned} \tag{3}$$

where the subscripts '*l*' and '*g*' represent liquid and gas properties respectively while α is the gas volume fraction.

Equations (1) and (2) are rewritten in a non-conservative form by moving the density time derivative terms to the right hand side of the equations:

$$\frac{\partial \rho_m u_i}{\partial x_i} = -\frac{\partial \rho_m}{\partial t} \tag{4}$$

$$\rho_m\frac{\partial u_i}{\partial t} + \frac{\partial \rho_m u_i u_j}{\partial x_j} = -u_i\frac{\partial \rho_m}{\partial t} - \frac{\partial p}{\partial x_i} + \frac{\partial}{\partial x_j}\left[\upsilon_m\left(\frac{\partial u_i}{\partial x_j} + \frac{\partial u_j}{\partial x_i}\right)\right] - \rho_m\delta_{i3}\frac{1}{\mathrm{F_r}^2} \tag{5}$$

Equations (4) and (5) are solved using DYNAFLOW's flow solver 3DYNAFS-VIS©. 3DYNAFS-VIS© is based on the artificial-compressibility method [12], in which an artificial time derivative of the pressure is added to the continuity equation (4) as

$$\frac{1}{\beta_c}\frac{\partial p}{\partial \tau} + \frac{\partial \rho_m u_i}{\partial x_i} = -\frac{\partial \rho_m}{\partial t} \tag{6}$$

where β_c is an artificial compressibility factor and τ is the pseudo-time. By replacing equation (4) with (6) , it forms a hyperbolic system of equations along with (5) and is solved using a time marching scheme in pseudo-time. Note that the time variation of density is enforced as a source term in equations (6) and (5). The equations are transformed to generalized curvilinear coordinates to perform complex geometry calculations. To obtain a time-dependent solution, a Newton iterative procedure with different pseudo-time stepping in τ at each physical time step t is used in order to satisfy the continuity equation.

The numerical scheme in 3DYNAFS-VIS© uses a finite volume formulation. A first-order Euler implicit difference formula is applied to the time derivatives. The spatial differencing of the convective terms uses the flux-difference splitting scheme based on Roe's method [13] and a van Leer's MUSCL method [14] for obtaining the first- or third-order fluxes. A second-order central differencing is used for the viscous terms. The flux Jacobians required in an implicit scheme are obtained numerically. The resulting system of algebraic equations is solved using a discretized Newton Relaxation method in which symmetric block Gauss-Seidel sub-iterations are performed before the solution is updated at each Newton interaction.

Note the density ρ_m in this methodology is not solved for but introduced through the knowledge of the bubble distribution from the Lagrangian solver. The variation in the density is determined by the actual bubble dynamics of the medium following the bubble dynamics model detailed in the subsequent section.

Lagrangian Bubble Dynamics Model

To model the two-phase medium, the multi-bubble dynamics and trajectory code, 3DYNAFS-DSM©, was applied to track the bubble nuclei and predict their dynamics. In 3DYNAFS-DSM© the bubble transport is modeled via a bubble motion equation [17], while the bubble dynamics is simulated by solving a Surface Averaged Pressure (SAP) modified Rayleigh-Plesset equation [18].

In the present study we have considered the following form of the equation for the bubble radius, $R(t)$, which accounts for liquid and gas compressibility, liquid viscosity, surface tension, and non-uniform pressure fields, and is based on the Keller-Herring approach [19]:

$$\left(1-\frac{\dot{R}}{c_m}\right)R\ddot{R} + \frac{3}{2}\left(1-\frac{\dot{R}}{3c_m}\right)\dot{R}^2 = \frac{\left(\mathbf{u}_{enc} - \mathbf{u}_b\right)^2}{4} + \frac{1}{\rho_m}\left(1+\frac{\dot{R}}{c_m} + \frac{R}{c_m}\frac{d}{dt}\right)\left[p_v + p_g - p_{enc} - \frac{2\gamma}{R} - 4\mu_m\frac{\dot{R}}{R}\right] \tag{7}$$

where c_m is the sound speed in the medium, ρ_m is the medium density, p_v is the vapor pressure, p_g is the gas pressure, R is the radius of the sphere, γ is the surface tension and μ_m is the medium viscosity. In Equation (7), we have accounted for a slip velocity between the bubble and the host liquid, and for a non-uniform pressure field along the bubble surface [18]. p_{enc}

and $\mathbf{u}_{enc}$ are defined as the average of the liquid pressures and velocities over the bubble surface. The use of p_{enc} results in a major improvement over the classical spherical bubble model which uses the pressure at the bubble center in its absence. The bubble trajectory is obtained using the following motion equation [15]:

$$\frac{d\mathbf{u}_b}{dt} = -\frac{3}{\rho_m}\nabla p - 2g + \frac{3}{4}\frac{C_D}{R}\left(\mathbf{u}_{enc} - \mathbf{u}_b\right)\left|\mathbf{u}_{enc} - \mathbf{u}_b\right| + \frac{3}{2\pi}\frac{C_L}{R}\sqrt{\frac{\mu_m}{\rho}}\frac{\left(\mathbf{u}_{enc} - \mathbf{u}_b\right)\times\boldsymbol{\omega}}{\sqrt{|\boldsymbol{\omega}|}} + \frac{3}{R}\left(\mathbf{u}_{enc} - \mathbf{u}_b\right)\dot{R} \quad (8)$$

where $\mathbf{u}_b$ is the bubble velocity, g is gravity, C_L is the lift coefficient, $\boldsymbol{\omega}$ is vorticity, and C_D is the drag coefficient given by an empirical equation such as that of Haberman & Morton [20]:

$$C_D = \frac{24}{R_{eb}}\left(1 + 0.197 R_{eb}^{0.63} + 2.6\times10^{-4} R_{eb}^{1.38}\right)$$
$$R_{eb} = \frac{2\rho R\left|\mathbf{u}_{enc} - \mathbf{u}_b\right|}{\mu} \quad (9)$$

The last term on the right hand side of equation.(8) is the force due to the bubble volume variations, which is obtained by solving equation (7).

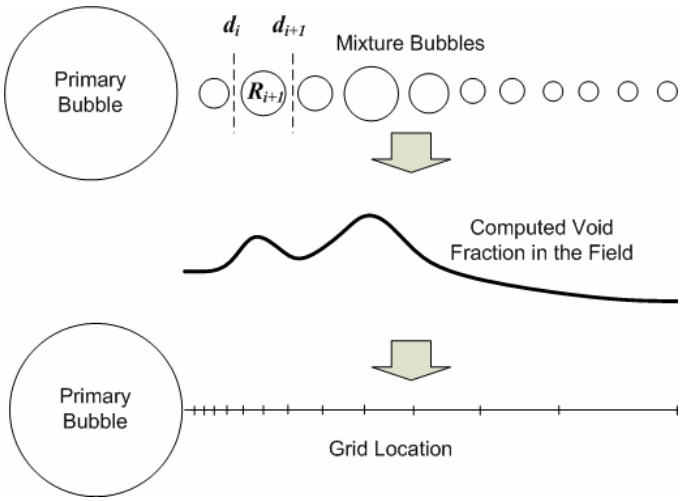

Figure 1: Schematic showing representative bubbles, the computed void fraction and its interpolation onto the computational grid.

Eulerian-Lagrangian Coupling

The coupling between the two-phase continuum flow model 3DYNAFS-VIS© and the Lagrangian 3DYNAFS-DSM© solver can be described as follows:

- The bubbles in the flow field are influenced by the two-phase medium local properties and gradients, and the dynamics and motion of the individual bubbles are based on these quantities,
- The local properties of the mixture are determined by the bubbles presence, and the void fractions and local densities are determined by the instantaneous bubbles distributions,
- The flow field adjusts itself to the evolving mixture density distribution while satisfying mass and momentum conservation.

Representative bubbles distributed in the radial direction to determine the local variations of the void fraction in the liquid. Each of these bubbles represents a group of m_f same sized bubbles located in a very small region around it. At each of these locations for the control volume $d\forall$, the void fraction α is calculated by:

$$\alpha = \sum \frac{4}{3}\pi m_f R_i^3 \Big/ \frac{4}{3}\pi\left(d_i^3 - d_{i-1}^3\right) \quad (10)$$

In the example shown in Figure 1, the representative bubbles are assumed to be of the same size R_i and one bubble representing m_f other bubbles are placed in the control volume $d\forall$. Here control volume dV is the volume formed by the mid-distance between the two adjacent bubbles, which in the above example, are d_i and d_{i+1}. The representative bubble assumption has two advantages; with this approach a uniform initial void fraction distribution can be obtained in the field and secondly, effect of different bubble sizes can be studied for the same initial void fraction. At each time step the void fraction is calculated at the bubble location and its radial variation in the field determined by a linear fit between these locations as shown in Figure 1 . This curve is then interpolated onto the grid to represent the spatial distribution of the α .

Eulerian Compressible Solver

The compressible flow calculations were carried out using the Eulerian finite difference solver, GEMINI, developed by the Naval Surface Warfare Center, Indian Head. GEMINI is based on the Gudonov scheme solved on a Cartesian grid and has been validated against several experimental data in the past [15,16].

For the current problem we have used the spherical version of the solver which solves the flow field in one dimension only.

ANALYTICAL MODEL

An equation governing the wall-motion dynamics of a spherical bubble in a compressible medium based on Gilmore's approach [19] can be written as follows:

$$\left(1 - \frac{\dot{R}}{c_m}\right)R\ddot{R} + \frac{3}{2}\left(1 - \frac{\dot{R}}{3c_m}\right)\dot{R}^2 = H\left(1 + \frac{\dot{R}}{c_m}\right) + \frac{R\dot{H}}{c_m}\left(1 - \frac{\dot{R}}{c_m}\right) \quad (11)$$

In the above equation, H is the enthalpy difference between the bubble surface and infinity.

$$H = \int_{P_\infty}^{P} \frac{dp}{\rho} \quad (12)$$

where P_∞ is the pressure at infinity and P is the pressure at the bubble wall. P can be expressed as follows:

$$P = p_v + p_{g0}\left(\frac{R_0}{R}\right)^{3k} - \frac{2\gamma}{R} - \frac{4\mu\dot{R}}{R} \tag{13}$$

where the gas inside the bubble is assumed to obey the polytropic compression law [21] of constant k, p_{g0} is the initial gas pressure inside the bubble – corresponding to a bubble radius of R_0.

If an equation describing the pressure-density relationship for the medium is known, the above equations can be solved to obtain the variation of bubble radius with time.

Pure Water

For pure water, the pressure-density relation for isentropic compression can be given by the Tait equation [22]:

$$\frac{p+B}{P_\infty + B} = \left(\frac{\rho}{\rho_\infty}\right)^n \tag{14}$$

ρ_∞ is a reference density corresponding to the pressure P_∞. B and n are constants ($B \approx 3000$ atm and $n \approx 7$ for water). Using (14), the sound speed at a point in the fluid domain can be expressed as follows:

$$c_m^2 = \frac{dp}{d\rho} = \frac{n(p+B)}{\rho} \tag{15}$$

Using (14) and (15), the sound speed C on the bubble surface can be expressed by the following relation:

$$C = c_\infty \left(\frac{P+B}{P_\infty + B}\right)^{\frac{n-1}{2n}} \tag{16}$$

In the above equation, c_∞ is the reference sound speed corresponding to the reference pressure P_∞. Similarly, using (12) and (14) , one may obtain the following expression for H :

$$H = \frac{n(P_\infty + B)}{(n-1)\rho_\infty}\left[\left(\frac{P+B}{P_\infty + B}\right)^{\frac{n-1}{n}} - 1\right] \tag{17}$$

Once H and C on the bubble surface are known, the system of equations describing the wall-motion dynamics of a spherical bubble can be solved.

Bubbly Medium

The sound speed in a compressible two phase medium can be expressed as follows [9];

$$c^2 = \frac{p}{\rho_l}\frac{\left[1+\frac{\alpha}{1-\alpha}\right]^2}{\left[\frac{1}{k}\frac{\alpha}{1-\alpha} + \frac{p}{\rho_l c_l^2}\right]} \tag{18}$$

where c_l the sound speed in pure liquid. In deriving the above relation, the following assumptions have been made

- the density of the gas phase, ρ_g, is much smaller than the density of the liquid phase, ρ_l, and is neglected in Equation (3).
- the disperse gas phase obeys the polytropic compression law.
- surface tension is absent at the interface of the two components (p varies smoothly in the medium) and,
- the void fraction, α, is small.

Equation (18) can be integrated to obtain the equation of state (relating pressure and density/void-fraction) for the bubbly medium 9:

$$\frac{\alpha}{1-\alpha} = \left[\frac{\alpha_0}{1-\alpha_0} + \frac{k}{k+1}\frac{p_0}{\rho_l c_l^2}\right]\left(\frac{p_0}{p}\right)^{\frac{1}{k}} - \frac{k}{k+1}\frac{p}{\rho_l c_l^2} \tag{19}$$

In the above equation, α_0 is a reference void-fraction corresponding to a reference pressure P_0. In our computations, we have assumed $P_0 = P_\infty$. Equation (19) and Equation (3)can be used to describe H on the bubble surface :

$$H = \frac{P - P_\infty}{\rho_l} + (A+B)\frac{k}{\rho_l(k-1)}p_0^{\frac{1}{k}}\left(P^{\frac{k-1}{k}} - P_\infty^{\frac{k-1}{k}}\right) - \frac{B}{2p_0\rho_l}\left(P^2 - P_\infty^2\right) \tag{20}$$

Also, note that for a given bubble wall pressure P, c on the bubble surface can be obtained using equations (18) and (19).

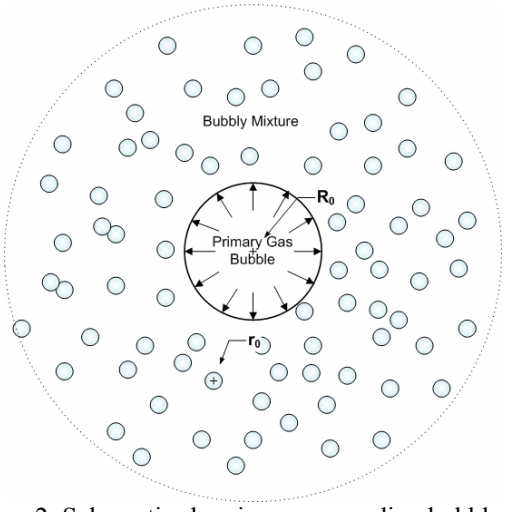

Figure 2: Schematic showing an expanding bubble in a homogeneous mixture.

PROBLEM SETUP

Eulerian-Lagrangian Setup

An expanding gas bubble of initial radius R_0 is placed within a bubbly mixture as seen in Figure 2. We assume that bubbles are uniformly distributed in the field and are of the same size. Similar problems have been studied in the past for the dynamics of spherical bubble clouds/clusters [9, 23, 24, 25]

under various conditions. The notable difference for the present setup is the presence here of the primary bubble which acts as the pressure perturbation source driver, which also responds to the dynamics of the surrounding bubbles. This interaction is expected to be highly non-linear.

For the 3DYNAFS-VIS© calculations we use an O-O type single block grid, as shown in Figure 3. The bubble surface is generated using 41 x 21 grid nodes while the field is resolved using 41 nodes in the radial location, clustered in the proximity of the bubble surface. Similar setup has been used in the past and validated against 3DYNAFS-BEM© potential solver based on the Boundary Element Method, [21]). To best describe the bubble surface behavior, a general free surface boundary condition satisfying both kinematic and dynamic boundary conditions is imposed [26].

The kinematic condition is that a particle on the surface remains on the surface. For a surface of equation $F(x_i,t)=0$, this can be written $DF/Dt=0$. The dynamic condition imposes zero shear stress (we ignore here stress generated by the air in the bubble) and balance of normal stresses at the interface. With the same simplifications used by Batchelor [27] for deriving the dynamic boundary condition in the Cartesian coordinate system, Hodges et al. [28] derived a dynamic boundary condition in a curvilinear coordinate system by requiring the grid to be normal to the boundary. For non-inertial curvilinear coordinates represented as (ξ,η,ζ), we follow their work with a further assumption that $\partial W/\partial\xi$ and $\partial W/\partial\eta$ are small and write the dynamic boundary condition at ζ=0, i.e. at the bubble surface. In non-dimensional form this becomes:

$$\left.\frac{\partial U}{\partial\zeta}\right|_{\zeta=0}=0 \tag{21}$$

$$\left.\frac{\partial V}{\partial\zeta}\right|_{\zeta=0}=0 \tag{22}$$

$$p=p_{gv}+\frac{2}{\mathrm{Re}}\left.\frac{\partial W}{\partial\zeta}\right|_{\zeta=0}-\frac{C_b}{\mathrm{We}_b} \tag{23}$$

where (*U, V, W*) are contravariant velocity components in the curvilinear coordinates and C_b is the curvature of the bubble interface.

$$\mathrm{We}_b=\rho u_{charc}^2 L/\gamma_b \tag{24}$$

is the Weber number with γ_b being the surface tension at the bubble interface. u_{charc} and L are a characteristic velocity and length, respectively. The term p_{gv} in Equation (23) is the non-dimensional pressure difference between the pressure inside the bubble and the reference pressure, P_∞

$$p_{gv}=(p_g+p_v-P_\infty)/\rho u_{charc}^2 \tag{25}$$

To determine the gas pressure we assume that the amount of gas inside the bubble remains constant and that the gas satisfies the polytropic relation:

$$p_g\forall^k=\text{constant} \tag{26}$$

where $\forall$ is the gas volume.

At the farfield boundary an extrapolated boundary condition is used. As the bubble expands and collapses the field grid is deformed using a combined algebraic and elliptic grid generation technique [29]. This grid generation scheme is selected because the algebraic grid generation technique is suited to create clustering and boundary-orthogonal grids at the bubble surface, which is important for resolving the flow field near the bubble surface and for applying appropriate free surface boundary conditions. The Elliptic grid generation technique is then applied to smooth out the rough algebraic grid. The farfield boundary is selected at a distance of 100 R_0 from the center of the bubble.

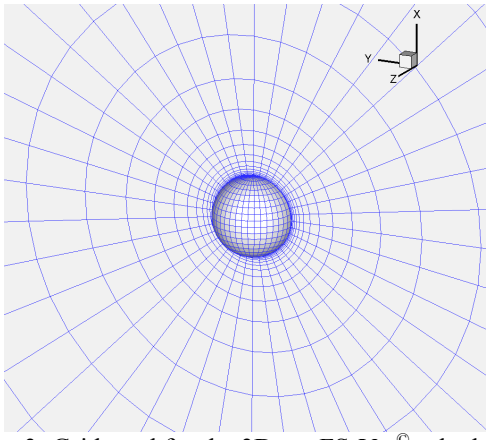

Figure 3: Grid used for the 3DYNAFS-VIS© calculations

Eulerian Setup

For the compressible computations using GEMINI, the bubbly medium is modeled as a homogeneous mixture of air and water. The primary bubble surface is represented using an interface capturing scheme in the spherical coordinates. Non-reflecting boundary conditions are used in the farfield located at a distance of 2,000 R_0 from the bubble center. We have used 648 grid points in the radial direction, which was found sufficient to capture the pressure characteristics for the current setup. Note that here unlike Eulerian-Lagrangian approach, the variation in void fraction is not determined by discrete bubbles. We compute the bubble dynamics in an *a posteriori* fashion using 3DYNAFS-DSM© using the same distribution used in the Eulerian-Lagrangian calculations.

RESULTS

As an example we consider a bubble with initial radius, R_0 = 0.005 mm and initial gas pressure, P_{g0} = 2 atm, twice the ambient pressure. The surrounding liquid is assumed to be water while the gas is assumed to be air. Gravity is neglected to conserve the spherical nature of the problem. The surrounding

bubbles are initially in equilibrium with the ambient conditions of the fluid. For the preliminary baseline calculations using the coupled Eulerian-Lagrangian calculations, as well as 3DYNAFS-DSM© only calculations, we have chosen the initial radius of the bubbly mixture nuclei to be r_0 = 1mm. Bubbly medium void fraction ranging from 0 – 0.25% have been tested with this setup.

Effect on Primary Bubble Radius

Figure 4 compares the primary bubble radii versus time for different void fractions up to α = 0.25% using the Eulerian-Lagrangian approach. Similar comparison is also shown for the multi-component compressible approach and using Gilmore's approach in Figure 5 and Figure 6, respectively.

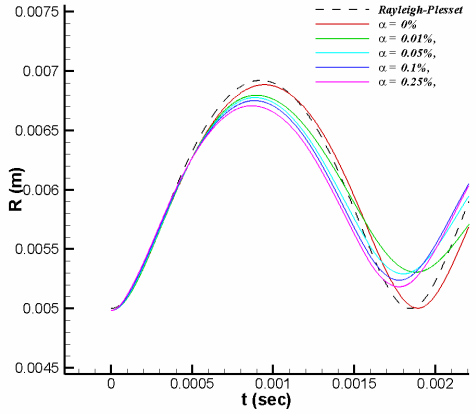

Figure 4: Variation of the primary bubble radius versus time for different void fractions for the Eulerian-Lagrangian calculations.

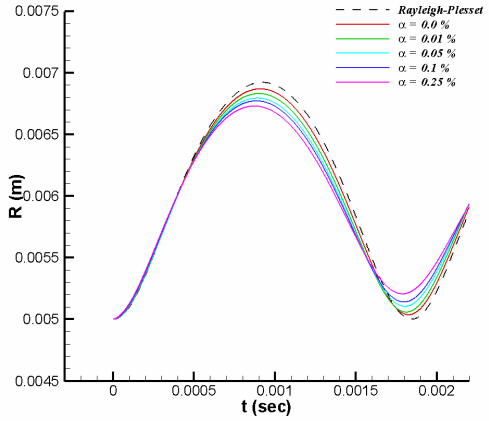

Figure 5: Variation of the primary bubble radius versus time for different void fractions for the multi-component compressible approach calculations.

The numerical solvers are also compared with the analytical approach using Rayleigh-Plesset [30] for the α = 0.0%. Note that, Equation (11) will revert to this form for incompressible fluids, i.e. $c \rightarrow \infty$. For the Eulerian approach the period of the primary bubble decreases as the surrounding void fraction increases while the minimum volume of the bubble at collapse increases, which is illustrated better in Figure 7 and Figure 8. This is different from the Eulerian-Lagrangian solution where the bubble volume at collapse does not seem to follow a clear trend from low to higher void fractions. This can be attributed to the highly nonlinear interaction of the bubble dynamics with the surrounding mixture due the discrete representation and warrants further investigation. The period of the bubble, on the other hand, does follow the decrease in period of bubble collapse. This illustrates that the presence of bubbly mixture can in fact impede the growth and collapse of expanding bubble. We will try to examine the cause for this phenomenon in the subsequent portion of this section. The analytical model can capture the increase in the minimum volume of collapse, but does not show significant change in the period of the bubbles at these void fractions, as seen in Figure 6, and later in Figure 8.

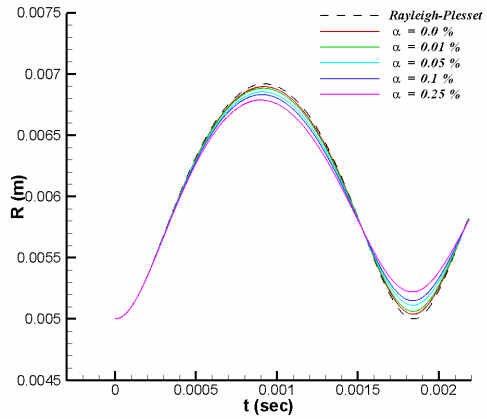

Figure 6: Variation of the prrimary bubble radius for different void fractions calculated using Gilmore's model.

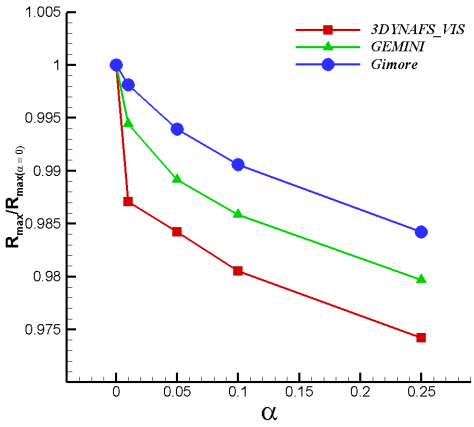

Figure 7: Comparison of normalized maximum radius R_{max} for the three approaches.

Figure 7 compares the maximum bubble radius for different void fractions for all three approaches normalized by the maximum bubble radius at $\alpha = 0.0\%$. All three approaches show that as the void fraction increases there is a corresponding decrease in the maximum bubble radius. Overall the Eulerian-Lagrangian shows a 2.5% reduction in the size of the primary bubble while the analytical approach shows nearly 1.6% reduction at the maximum void fraction. Similar comparison is also shown for different void fractions for the period of the bubble, normalized by the bubble period at $\alpha = 0.0\%$ in Figure 8. There is a significant difference in bubble period between the three approaches. The analytical model shows a marginal change in the bubble period while the Eulerian-Lagrangian approach shows that the bubble period decreases by nearly 6% at $\alpha = 0.25\%$ and the multi-component compressible approach shows a 2% decrease.

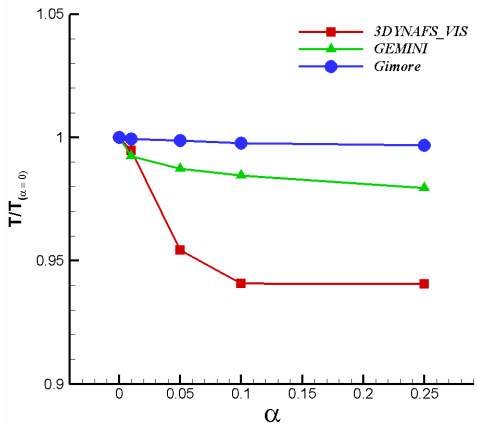

Figure 8: Comparison of normalized bubble period for the three approaches.

Field Pressure Variation

Figure 9, Figure 10 and Figure 11 show the pressure variation in time for a point in the field at $r = 7$ mm for all the three models. It is clearly seen that the presence of the bubbly mixture tends to dampen the pressure wave propagation in the field with the highest void fraction causing the maximum attenuation. For the Eulerian-Lagrangian approach with the increase in the void fraction in the field, the pressure starts showing small oscillations, as seen in Figure 9 near the minimum pressure. This can be attributed to the presence of discrete bubbles in the field which causes localized changes in the void fraction due to the presence of discrete bubbles altering the pressure wave propagation through the medium. This is further illustrated in Figure 14 later. For the other two solvers, however, since the medium is represented by a homogeneous mixture the pressure shows a smooth curve. Note that the jump seen in the pressure for the multi-component compressible approach calculations in Figure 10 are due to the initial pressure generated at the initiation of the computations. For the Eulerian-Lagrangian approach a sharp drop in pressure is seen initially for $\alpha = 0.25\%$, which could be due to a strong interaction between the primary and surrounding bubbles.

The pressure wave variations in time for the three approaches are compared in Figure 12 and Fig. 13 for the α=0.0% and α=0.25% respectively. In the pure liquid the pressure peak at the bubble collapse is of the same magnitude as the initial pressure peak and comparable with the pressure obtained using Rayleigh-Plesset solution for a pure liquid. The difference in the period for the three approaches is seen which requires further analysis. For $\alpha = 0.25\%$ all three approaches demonstrate that field pressure is attenuated indicating the bubble loses energy due the presence of bubbly medium. The differences between the three approaches is however of the same order as the differences for the pure liquid.

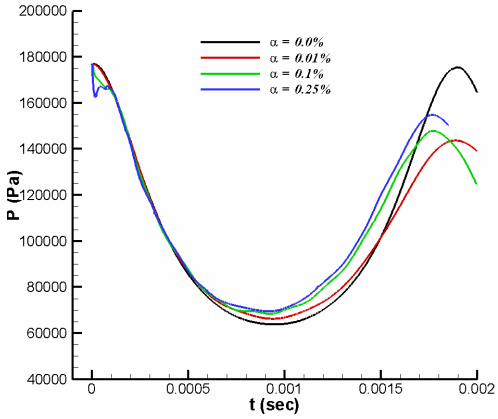

Figure 9: Variation of the pressure at $r = 7$ mm for different void fractions for the Eulerian-Lagrangian approach.

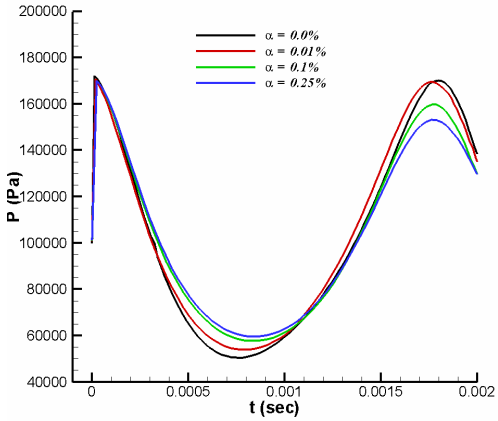

Figure 10: : Variation of the pressure at $r = 7$ mm for different void fractions for the multi-component compressible approach calculations.

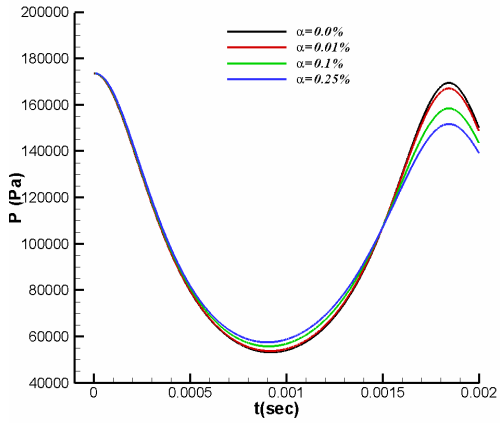

Figure 11: Variation of the pressure at r = 7 mm for different void fractions calculated using Gilmore's model.

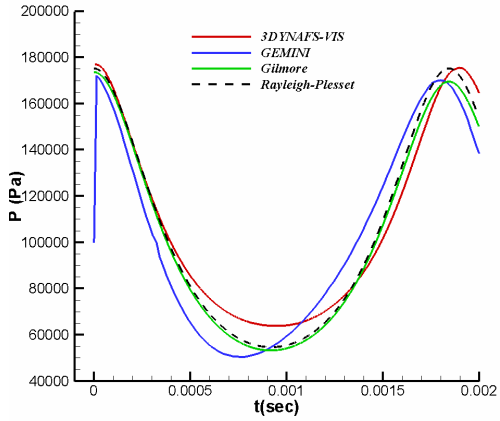

Figure 12: Comparison of the time variation of the pressure at r = 7 mm for α = 0.0% for the three approaches.

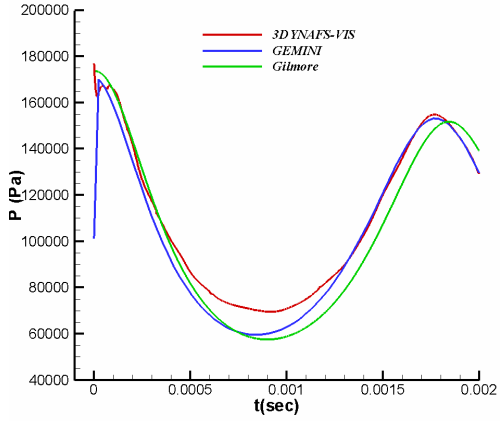

Fig. 13: Comparison of the time variation of the pressure at r = 7 mm for α = 0.25% for the three approaches.

The differences between the three approaches are further examined by analyzing the variation of both void fraction and pressure in the field at different locations. Figure 14 shows the time pressure variations for three different locations and the corresponding variations of the local void fraction for the Eulerian-Lagrangian calculations. Here, the locations r = 7 mm, 15 mm and 400 mm correspond to locations near the bubble surface, near field and in the farfield respectively. Due to the high pressure variations encountered by the bubbles near the bubble surface, the void fraction in this region shows the largest variations corresponding to the oscillations of the bubbles. However since the pressure wave is the strongest in this region, the effect of the presence of bubbles is less obvious. In the near field region further away from the bubble surface the void fraction oscillations are still strong and are more visible in the pressure variation. These oscillations in void fractions are similar to the experimental observations for a spark bubble in bubbly medium presented in the companion paper [31].

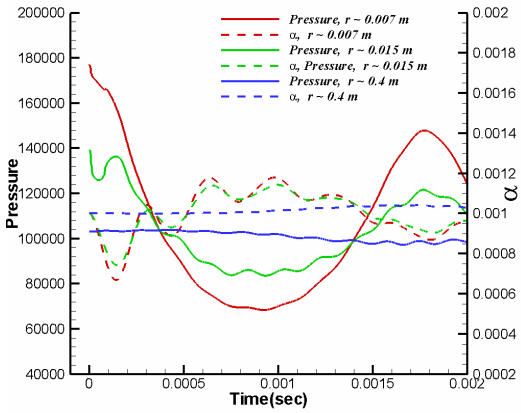

Figure 14: Variation of pressure and void fraction in the field with α = 0.1% for the Eulerian-Lagrangian calculations, at r = 7, 15 and 400 mm.

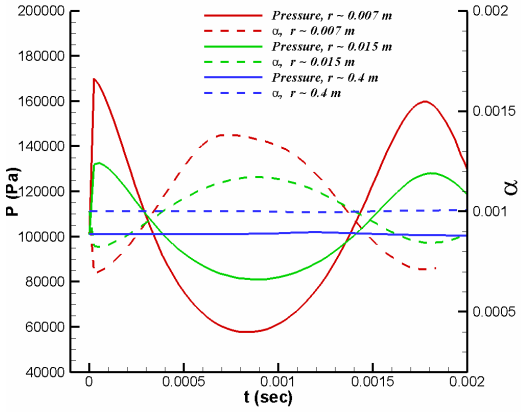

Fig. 15: Variation of pressure and void fraction in the field with α = 0.1% for the multi-component compressible approach calculations., at r = 7, 15 and 400 mm.

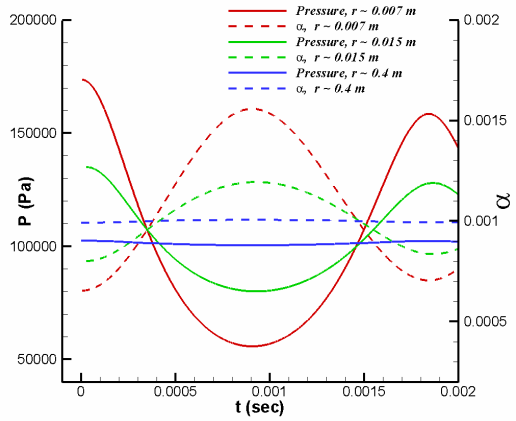

Figure 16: Variation of pressure and void fraction in the field with $\alpha = 0.1\%$ calculated using the analytical Gilmore model., at $r = 7$, 15 and 400 mm.

For the multi-component compressible approach and Gilmore approaches, due to the homogeneous mixture assumption, the variation of the void fractions at these locations are relatively smooth, seen Fig. 15 and Figure 16. Near the primary bubble surface, the analytical model predicts a slightly higher change in void fraction corresponding to the maximum bubble radius than the multi-component compressible approach solver. The latter predicts a peak value of around $\alpha = 0.14$ % while Gilmore model predicts around $\alpha = 0.16$ %; for the same location the Eulerian-Lagrangian solver predicts peak values around 0.12% only, as seen in Figure 14.

Void Fraction Variations

Figure 17(a) compares the void fraction distribution in space at different time instances for the Eulerian-Lagrangian approach during the initial growth of the bubble. Similar comparison during the collapse of the bubble is shown in Figure 17(b). During the initial growth of the primary bubble there is a decrease in medium bubble sizes leading to a decrease in the void fraction. Subsequently, however, as the field pressure drops but not in phase the bubbles rebound and lead to an increase in the void fraction. There is marked difference in the dynamics of bubbles near the surface than ones in the farfield. Near the surface, there is a rapid change in the void fraction which changes in the radial direction due to a phase shift between the bubbles in the field. Similar observations are made during the collapse phase of the primary bubble. A larger region of increased void fraction is seen in the field towards the end of the collapse extending from nearly, $r =$ 50 mm to 350 mm.

The void fraction distribution in the field for all the three approaches is compared in Figure 18, at different time instances of the bubble period, T. During the growth of the bubble both homogeneous mixture approaches match very well, while the Eulerian-Lagrangian one, due to the large oscillations of the bubbles in the proximity of the bubble surface, has a localized change in the void fraction in that region. When the primary bubble reaches its maximum radius the void fraction near the bubble surface increases by 40%, then it decreases monotonically as the radial direction increases. In comparison the Eulerian-Lagrangian approach shows similar trend with a lower values as was also observed in Figure 14. At around 3/4 of the bubble period the Eulerian approach and analytical Gilmore model show a slight phase shift.

As mentioned earlier, while for the Eulerian-Lagrangian approach, the void fraction dips near the bubble surface, further away at around $r = 0.1$ m, the void fraction is higher indicating that the bubbles in this region are in the growth phase while those near the bubble surface are shrinking. This is not caught by the homogeneous approached. This is an important deviation between the two approaches and can be attributed to the non-linear nature seen in the Eulerian-Lagrangian approach.

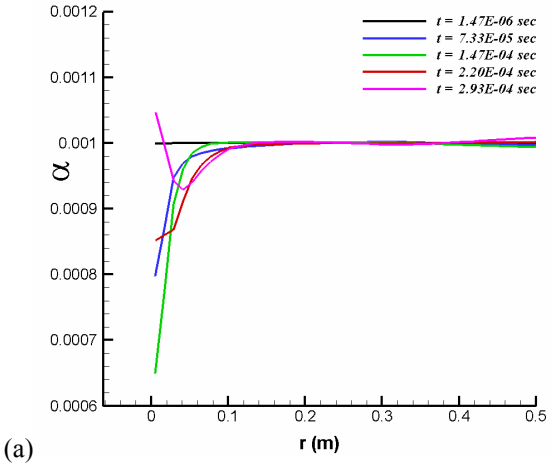

(a)

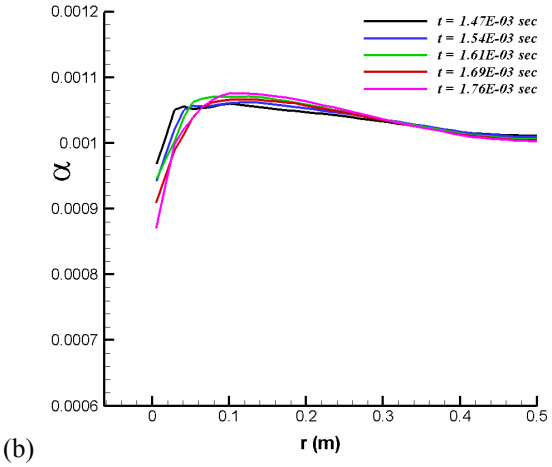

(b)

Figure 17: Comparison of the change in void fraction in the field during the (a) growth and (b) collapse phase of the primary bubble for the Eulerian-Lagrangian calculations.

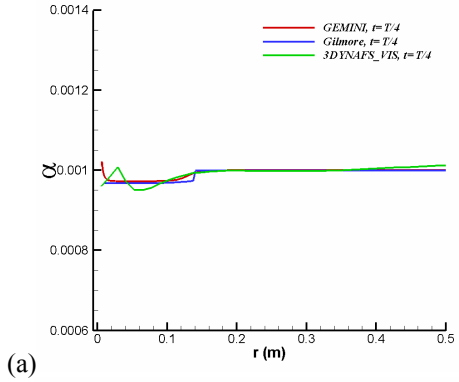

(a)

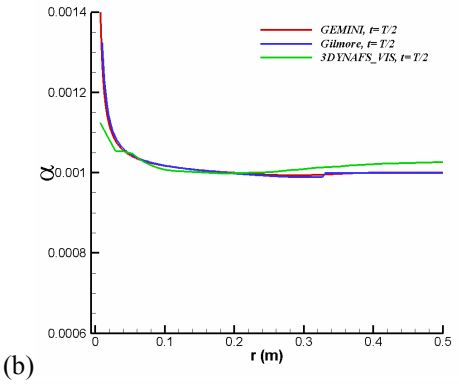

(b)

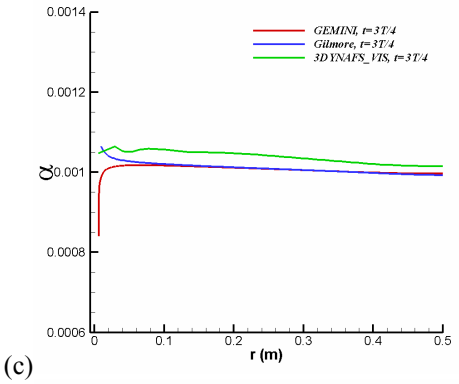

(c)

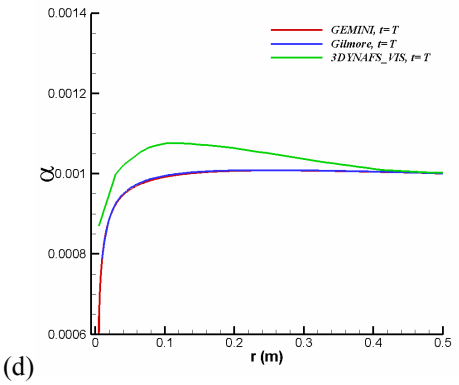

(d)

Figure 18: Comparison of the void fraction in the field for the different approaches at different phase of the bubble period.

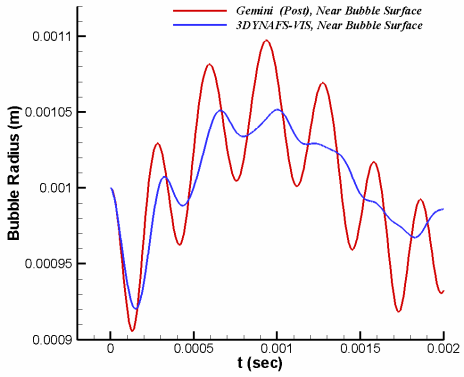

(a)

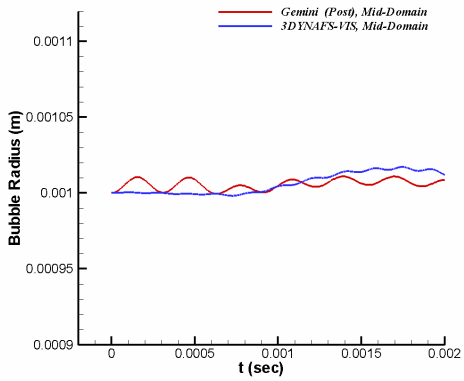

(b)

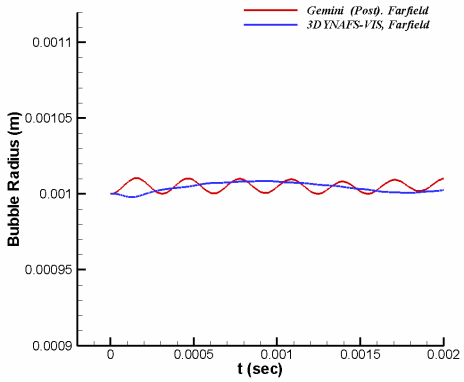

(c)

Figure 19: Comparison of the bubble radius in the field at three different locations for two-way and one-way coupled approaches.

Mixture Bubble Dynamics

Figure 19 compares the changes in the mixture bubble radius over the period of the primary bubble for two different approaches. The two-way coupling refers to the Eulerian-Lagrangian approach calculations while the one-way coupling refers to Lagrangian calculations carried out *a posteriori* with the multi-component compressible approach solution. Bubbles at three different locations are examined and it is observed that

for one-way coupling calculations the bubbles tend to oscillate with a higher magnitude than the two-way coupled bubbles specifically near the bubble surface. This is attributed to the coupling where changes in the void fraction effect the local field and are "felt" by the discrete bubbles changing its subsequent behavior while for one-way coupling the localized changes in the homogeneous medium are relatively smooth as observed in Figure 18. One can observe both cases show a global time scale which is the result of the pressure in the field. On the other hand, the bubble time scale seems to be about the same between the two methods.

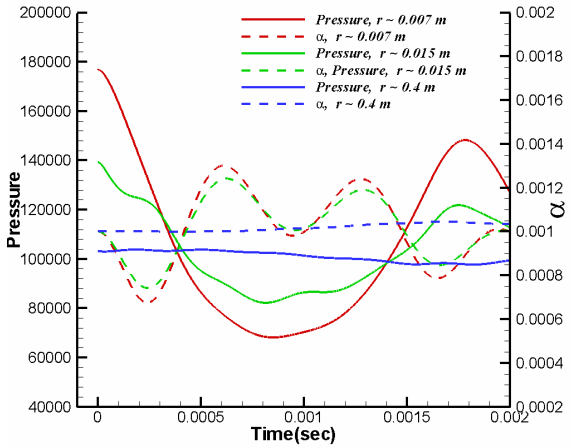

Figure 20: Variation of pressure and void fraction in the field for $\alpha = 0.1\%$ and $r_0 = 2$mm, for Eulerian-Lagrangian calculations.

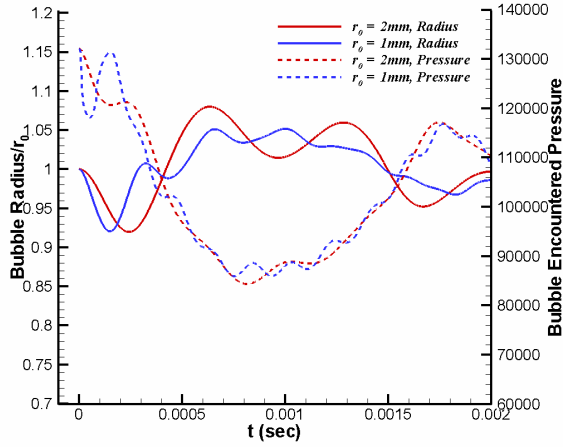

Figure 21: Variation of mixture bubble radius and the pressure it encounters for the first bubble in the bubbly medium for two different initial sizes with $\alpha = 0.1\%$, for Eulerian-Lagrangian calculations.

Effect of Changing Mixture Bubble Size

The size of the nuclei in the bubbly mixture are expected to play an importrant role in the solution even if the initial void fraction is conserved, For this reason, another set of simulation with $\alpha = 0.1\%$ and $r_0 = 2$mm was conducted with the Eulerian-Lagrangian approach. Figure 20 shows the pressure and the void fraction variations in the field. It can be observed that with the increase in the size of the bubbles, the period of oscillations of the void fraction as well as its amplitude increases as compared to the baseline case seen in Figure 14.

The variations in size of the medium bubbles close to the bubble surface along the pressure seen by it are compared in Figure 21. This follows the observed trend with the larger bubbles oscillating with a larger amplitude and period directly effecting the local void fraction variations. The field pressure seen by the bubble shows the effect of the oscillations due to changes in void fraction as well as the due to the translation of the bubble itself in the field.

CONCLUSION

We have conducted simulations to study strong pressure oscillations in a bubbly medium using three different approaches. The effect of the presence of discrete bubbles in a liquid is studied using 3DYNAFS-VIS©, an Eulerian solver coupled with a Lagrangian discrete bubble dynamics solver. The significance of using a homogenous mixture instead of discrete bubbles is also studied using a compressible solver GEMINI as well as an analytical model based on Gilmore's approach.

For the pressure due to a primary expanding gas bubble in a bubbly medium we find that the presence of discrete bubbles leads to a non-linear phenomenon in the flow. The presence of the bubbly medium tends to impede the growth and collapse of the primary bubble. Although the Eulerian and analytical Gilmore approaches match very well at the tested void fractions, the coupled runs indicate changes in the local void fraction due to the discrete bubble dynamics. These local changes cause perturbations in the pressure distribution in the field which are not captured when using the homogeneous mixture assumption. For the cases tested, these perturbations are also found to be a function of the bubble sizes in the field.

ACKNOWLEDGEMENT

This work was supported by the Department of Energy under contract DE-FG02-07ER84839. The authors would also like acknowledge support from the Office of Naval Research under contract N00014-09-C-0676 monitored by Dr. Ki-Han Kim.

NOMENCLATURE

B	Constant
C	Sound speed on bubble surface
C_b	Curvature of the bubble interface
C_D	Drag coefficient

C_L	Lift coefficient
$\mathrm{F_r}$	Froude number
H	Enthalpy difference
L	Characteristic Length
P	Pressure at bubble wall
P_∞	Pressure at infinity
R	Bubble radius
R_e	Reynolds number
U, V, W	Contravariant velocity components
$\forall$	Gas volume
We_b	Weber number
c	Sound speed of medium
c_∞	Reference sound speed
d	mid-distance between bubbles
$d\forall$	Control volume
g	Gravity
k	Polytropic gas constant
m_f	Multiplication factor
n	Constant
p	Pressure
p_v	Vapor pressure
t	Time
u	Velocity
u_{charc}	Characteristic velocity
x	Directional vector
α	Void fraction
β_c	Artificial compressibility factor
γ	Surface tension of compressible medium
γ_b	Surface tension at the bubble interface
$\boldsymbol{\omega}$	Vorticity
ρ	Density of the medium
ρ_∞	Reference density
μ	Absolute Viscosity
υ	Kinematic Viscosity
τ	Pseudo-time
ξ, η, ζ	Curvilinear coordinates

Subscripts

0	Initial condition
b	Bubble property
enc	Average property on bubble surface
i, j, k	Indices
g	Gas property
l	Liquid property
m	Mixture property

REFERENCES

1. Crowe, C.T., Troutt, T.R. and Chung, J. N. , 1996, "Numerical Models for Two-Phase Turbulent Flows", Annual Review of Fluid Mechanics, **28**, pp.11-43.
2. Balachandar, S. and Eaton, J. K., 2010, "Turbulent Dispersed Multiphase Flow", Annual Review of Fluid Mechanics, **42**, pp. 111-133.
3. Elghobashi,S. E. , 1994, "On predicting particle-laden turbulent flows," Applied Scientic Research , **52**, pp. 309.
4. Apte S.V., Mahesh, K., and Lundgren, T., 2008 , "Accounting for finite-size effect in disperse two-phase flow", International Journal of Multiphase Flow, **34**(3), pp. 260-271.
5. Spelt, P. D. M and A. Biesheivel, A., 1997, "On the motion of gas bubbles in homogeneous isotropic turbulence," Journal of Fluid Mechanics, **336**, pp. 221-244.
6. Druzhinin, O. A. and Elghobashi,S. E. , 1998, "Direct numerical simulations of bubble-laden turbulent flows using the two-fluid formulation," Physics of Fluids, **10**, pp. 685.
7. Bunner, B. and Tryggvason, G., 2003, "Effect of bubble deformation on the stability and properties of bubbly flows", Journal of Fluid Mechanics, **495**, pp. 77–118.
8. Esmaeeli, A. and Tryggvason, G. , 1998, "Direct numerical simulations of bubbly flows. Part 1. Low Reynolds number array", Journal of Fluid Mechanics, **377**, pp. 313-345.
9. Brennen, C. E., 1995, *Cavitation and Bubble Dynamics*, Oxford University Press.
10. Van Wijngaarden, L. , 1964, "On the Collective Collapse ofa Large Number of Gas Bubbles in Water", Proceedings 11th International Congress of Applied Mechanics, Springer, Berlin, pp.854-861.
11. Prosperetti, A. , Sundaresan,S. , Pannala, S. and Zhang, D.Z. , 2007, "Segregated methods for two-fluid models," in Computational methods for multiphase flow, Cambridge University Press, pp. 320-385.
12. Chorin, A. J. , 1967, "A Numerical Method for Solving Incompressible Viscous Flow Problems," Journal of Computational Physics, **2**, pp. 12-26.

13. Roe, P. L. , 1981, “Approximate Riemann Solvers, Parameter Vectors, and Difference Schemes,” Journal of Computational Physics, **43**, pp. 357-372.

14. Van Leer, B., Thomas, J.L., Roe, P.L. and Newsome, R.W. , 1987, “A Comparison of Numerical Flux Formulas for the Euler and Navier-Stokes Equation,” AIAA Paper No. 87-1104-CP.

15. Wardlaw, A., Jr. and Luton J.A., 2000, “Fluid-Structure Interaction for Close-in Explosions”, Shock and Vibration Journal, **7**, pp.265-275.

16. Wardlaw, A., Jr., Luton J.A., Renzi, J. J. and Kiddy, K. , 2003, “Fluid-structure coupling methodology for undersea weapons”, Fluid Structure Interaction II, WIT Press, pp. 251–263.

17. Johnson, V.E. and Hsieh, T. , 1966, “The Influence of the Trajectories of Gas Nuclei on Cavitation Inception,” Sixth Symposium on Naval Hydrodynamics, pp. 163-179.

18. Hsiao, C.-T., Chahine, G. L. and Liu, H.-L. , 2003, “Scaling Effects on Prediction of Cavitation Inception in a Line Vortex Flow”, Journal of Fluid Engineering, **125**, pp.53-60.

19. Gilmore, F. R. , 1952, “The growth and collapse of a spherical bubble in a viscous compressible liquid,” California Institute of Technology, Hydro. Lab. Report 26-4.

20. Haberman, W.L. and Morton, R.K. , 1953, “An Experimental Investigation of the Drag and Shape of Air Bubbles Rising in Various Liquids,” Report 802, DTMB.

21. Chahine, G.L., Perdue, T.O., and Tucker, C.B. , 1988, “Interaction between an Underwater Explosion Bubble and a Solid Submerged Structure”, DYNAFLOW, INC., Technical Report 89001-1.

22. Dymond, J. H. and Malhotra,R. , 1988, "The Tait equation: 100 years on”, International Journal of Thermophysics, **9**(6), pp. 941-951.

23. Morch, K.A. , 1981, “Cavity cluster dynamics and cavitation erosion,” Proc. ASME. Cavitation and Polyphase Flow Forum, pp. 1-10.

24. Chahine, G. L., 1983, “Cloud Cavitation: Theory,” Proc. 14th Symposium on Naval Hydrodynamics, Ann Arbor, Michigan, National Academy Press, pp. 165-194.

25. Chahine, G. L. and Liu, H.-L., 1985, “A Singular Perturbation Theory of the Growth of a Bubble Cluster in a Superheated Liquid,” Journal of Fluid Mechanics, **156**, pp. 257-279.

26. Hsiao, C.-T. and Chahine, G.L. , 2001, “Numerical Simulation of Bubble Dynamics in a Vortex Flow Using Navier-Stokes Computations and Moving Chimera Grid Scheme,” Fourth International Symposium on Cavitation, California Institute of Technology, Pasadena, CA, June 20-23.

27. Batchelor, G.K., 1967, *Fluid Dynamics*, Cambridge University Press.

28. Hodges, B. R. , Street, R. L. and Zang, Y. , 1996, “A method for simulation of viscous, nonlinear, free-surface flows,” 20th Symposium on Naval Hydrodynamics, pp. 791-809.

29. Hsiao, C.-T. , 1996, “Numerical study of the Tip Vortex Flow over a Finite-Span Hydrofoil,” Ph.D. Thesis, Department of Mechanical Engineering, The Pennsylvania State University.

30. Plesset, M.S. and Prosperetti, A. , 1977, "Bubble Dynamics and Cavitation," Annual Review of Fluid Mechanics, **9**, pp.145-185.

31. Jayaprakash, A., Singh, S., and Chahine, G. L. , 2010, "Bubble Dynamics in a Two-Phase Bubbly Mixture", IMECE2010-40509, ASME 2010 International Mechanical Engineering Congress & Exposition, Vancouver, British Columbia, November 10-12.